Magnetic structure of $GdNi_2B_2C$ by resonant and nonresonant x-ray scattering

C. Detlefs, A. I. Goldman, C. Stassis, P. C. Canfield, and B. K. Cho
Ames Laboratory and Department of Physics and Astronomy, Iowa State University, Ames, Iowa 50011

J. P. Hill and D. Gibbs
Department of Physics, Brookhaven, National Laboratory, Upton, New York 11973

(Received 8 August 1995)

Resonant and nonresonant x-ray magnetic scattering techniques have been used to study the low-temperature magnetic structure of $GdNi_2B_2C$. Taken together, these measurements allow a determination of the ordered moment direction and its evolution with temperature from a single orientation of the sample. The experimental results show that below approximately 19.4 K this compound forms an incommensurate antiferromagnetic state with a magnetic wave vector of approximately $0.55\mathbf{a}^\star$ ($\mathbf{b}^\star$) in the basal plane of the tetragonal structure. Between 19.4 and 13.6 K, the ordered moment is along the **b** (**a**) axis. Below approximately 13.6 K an ordered component of the moment develops along the **c** axis.

I. INTRODUCTION

The study of the physical properties of the recently discovered[1–5] superconducting rare-earth nickel boride carbides RNi_2B_2C (R = rare earth) can provide further insight into the interplay between superconductivity and magnetism. The structure of these compounds is tetragonal (space group $I4/mmm$), consisting of RC layers separated by Ni_2B_2 sheets.[3] Superconductivity has been reported in these compounds not only for the nonmagnetic rare-earth elements, but also for some magnetic rare-earth elements including Tm (T_C = 10.8 K),[6] Er (T_C = 10.5 K),[7] Ho (T_C = 8.5 K),[8] and, most recently, Dy (T_C = 6.2 K).[9] Previous neutron diffraction studies of the magnetic structure of superconducting members of the RNi_2B_2C family including $HoNi_2B_2C$,[10,11] $ErNi_2B_2C$,[12,13] and $DyNi_2B_2C$ (Ref. 14) have also been reported.

For $HoNi_2B_2C$,[10,11] below approximately 4.7 K, the Ho moments are ordered in a simple antiferromagnetic structure. The moments are aligned ferromagnetically in each basal plane layer with the magnetic moments of two consecutive layers aligned in opposite directions. The most interesting result of these studies, however, was the appearance of a transient incommensurate magnetic phase, characterized by two magnetic wave vectors, $\mathbf{q}_a = 0.585\mathbf{a}^\star$ and $\mathbf{q}_c = 0.915\mathbf{c}^\star$, in the narrow temperature range between 4.7 and 6 K. It was suggested[10] that pair breaking associated with the transient magnetic structure(s) may be responsible for the deep minimum in H_{c2} and the almost reentrant behavior observed in this compound at approximately 5 K.[5,15,16] In $DyNi_2B_2C$,[14] below 10 K, the moments order in the simple antiferromagnetic structure found in the Ho-based compound at low temperature. Finally, in $ErNi_2B_2C$,[12,13] below 6 K, the moments order in an incommensurate modulated structure with wave vector $\mathbf{q}_a = 0.553\mathbf{a}^\star$, similar to one of the transient ordered structures found in the Ho-based compound.

For all of the above members of the RNi_2B_2C family, superconductivity coexists with magnetic ordering over some temperature range.[17] In addition, there are substantial crystal electric field (CEF) effects.[7,15,17,18] It is, therefore, also interesting to investigate the magnetic structures present in members, such as $GdNi_2B_2C$, which order in the absence of superconductivity. Band structure calculations[19] of the generalized susceptibility $\chi(\mathbf{q})$ for $LuNi_2B_2C$ show a pronounced peak for a wave vector of approximately $0.6\mathbf{a}^\star$ (or, equivalently, $0.6\mathbf{b}^\star$). These calculations suggest that the modulated structure with the wave vector along $\mathbf{a}^\star$ ($\mathbf{b}^\star$) and magnitude close to 0.6 is a common feature of these compounds and can be attributed to a nesting feature of their Fermi surfaces. Within this group of compounds, $GdNi_2B_2C$ is most likely to order with wave vectors consistent with the $\chi(\mathbf{q})$ calculations, due to the absence of the aforementioned CEF effects.

In this paper, we report the results of x-ray resonant exchange scattering[20,21] (XRES) and nonresonant[22–24] x-ray magnetic diffraction measurements on $GdNi_2B_2C$. While this compound is not superconducting above T = 2 K, it presents interesting behavior below its magnetic ordering temperature.[25] Specifically, magnetization measurements on powder samples exhibit a single phase transition at about 20 K to a magnetic state, while the measurements on oriented single crystals show two distinct transitions, the first at $T_N \approx 20$ K and the second at $T_R \approx 14$ K, as shown in Fig. 1. The polycrystalline average, $\chi_{\text{poly}} = 1/3\chi_{H\|c} + 2/3\chi_{H\perp c}$, of the single-crystal data is in good agreement with the powder measurements, suggesting that the transition at about 14 K arises from a spin reorientation that preserves the sublattice magnetization.[25] An overall decrease of the magnetic ordering temperatures was observed when Co was substituted for Ni.[26]

For this particular system, x-ray magnetic scattering measurements offer distinct advantages over the more common neutron diffraction techniques. First of all, since natural Gd

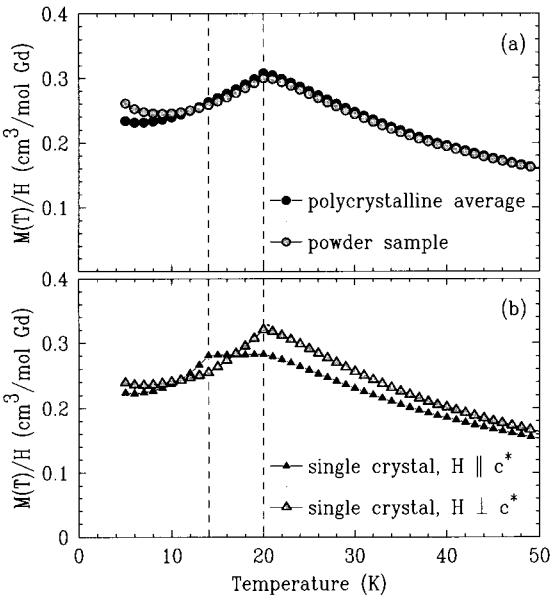

FIG. 1. (a) The magnetization data taken on powdered single-crystal samples are in good agreement with the polycrystalline average over the two single-crystal measurements with $\mathbf{H} \parallel \mathbf{c}$ and $\mathbf{H} \perp \mathbf{c}$, respectively. The antiferromagnetic ordering at the Néel temperature $T_N \approx 20$ K is clearly visible. (b) The single-crystal magnetization data reveal a second phase transition at $T_R \approx 14$ K. The constant susceptibility for $\mathbf{H} \parallel \mathbf{c}$ between the two transitions suggests that, in this temperature range, the magnetic moments are perpendicular to the **c** axis. The dashed lines indicate the two transition temperatures.

strongly absorbs neutrons, a very costly substitution of the nonabsorbing isotopes ^{156,158,160}Gd would be necessary for neutron measurements. Second, the order-of-magnitude increase in the **Q** resolution afforded by x-ray measurements at synchrotron sources allows a more detailed investigation of the behavior of the magnetic structure over large (several micrometer) length scales. Indeed, very recent XRES studies of $HoNi_2B_2C$ have shown that the magnetic structure in the intermediate temperature range, between 4.7 K and about 6 K, is considerably more complex than was previously realized.[27] Finally, as detailed below, the resonant and nonresonant x-ray scattering cross sections have different sensitivities to the spatial components of the ordered moment.[24,28] The measurement of both allows a more complete picture of the magnetic structure and its evolution with temperature to be determined from a single scattering geometry without reorientation of the sample.

Our experiments show that below $T_N = 19.4$ K $GdNi_2B_2C$ undergoes a transition to an incommensurate magnetic state characterized by a wave vector $\mathbf{q}_a = 0.55\mathbf{a}^\star$ $(0.55\mathbf{b}^\star)$, similar to the in-plane incommensurate ordering found in the Ho- and Er-based compounds.[10–13] Between 19.4 K and 13.6 K, the direction of the ordered magnetic moment is along the **b**(**a**) axis. As the temperature is lowered, the magnetic wave vector decreases continuously from 0.551 reciprocal lattice units (r.l.u.) to 0.550 r.l.u. until, at approximately 13.6 K, it starts to increase. At 3.5 K, the lowest temperature reached in this experiment, the wave vector of the modulation was determined to be 0.553 r.l.u. This

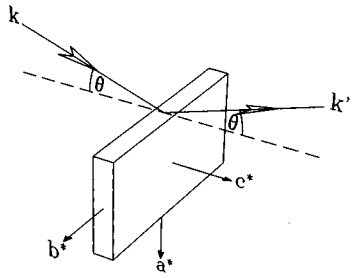

FIG. 2. The scattering geometry used in the present measurements with respect to the **a**, **b**, and **c** axes of the sample, using the convention of Blume and Gibbs (Ref. 24). The incident x-ray polarization is directed out of the scattering plane (σ polarization), along the **b** axis.

rather dramatic reversal in direction of the temperature dependence of the wave vector is coincident with the appearance of a component of the ordered moment along the **c** axis.

II. EXPERIMENTAL DETAILS

Single crystals of $GdNi_2B_2C$ were grown at the Ames Laboratory using a high-temperature flux growth technique.[15,7] Platelets extracted from the flux were examined with x rays and were found to be single crystals of high quality with the **c** axis perpendicular to their flat surface. Magnetization measurements as a function of temperature and magnetic field were performed using a Quantum Design superconducting quantum interference device (SQUID) magnetometer on single crystals from the same batch as those used in the x-ray experiments. The details of these measurements have been reported elsewhere.[25] One edge of the sample (perpendicular to one of the in-plane axes) was mechanically polished to remove any residual flux from the surface and to obtain a flat surface for x-ray diffraction. After polishing, the crystal was annealed at 900 °C in a vacuum of 10^{-7} torr for 36 h. The sample dimensions after polishing were approximately $4\times3\times0.75$ mm^3.

The synchrotron experiments were carried out at the bending magnet beamline X22C of the National Synchrotron Light Source, using a Ge(111) double crystal monochromator and an asymmetric cut Ge(111) analyzer. A Ni-coated toroidal focusing mirror upstream of the monochromator was used to eliminate higher harmonics in the incident beam. The sample was mounted on the cold finger of a Heliplex closed cycle refrigerator (base temperature 3.5 K) and oriented so that the $(h0l)$ zone was coincident with the vertical scattering plane of the diffractometer (Fig. 2). The mosaic spread of the $(h00)$ reflections was characterized by a full width at half maximum (FWHM) of 0.06°.

The resonant scattering technique[20,21] utilizes atomic absorption edges to obtain large enhancements in the magnetic scattering cross section. For the sample orientation shown in Fig. 2, and the incident x-ray beam linearly polarized perpendicular to the scattering plane, the XRES cross section for dipole transitions (i.e., $2p \leftrightarrow 5d$) may be related to the components of the magnetic moment in the scattering plane[28] by

$$I \propto \frac{(M_a \sin\theta - M_c \cos\theta)^2 \sin\theta}{\sin 2\theta}, \qquad (1)$$

where M_a and M_c represent the components of the magnetic moment along the **a** and **c** axes, respectively, and 2θ is the Bragg angle. The Lorentz factor, $1/\sin 2\theta$, as well as an angular factor required to correct for the fraction of the incident beam intercepted by the edge of the sample, $\sin\theta$, are included to allow a comparison between the calculated cross section and the measured integrated intensity I. Equation (1) contains only the angular dependence of the polarization factors. Although there is no magnetic form factor in the usual sense, it is conceivable that the matrix elements of the transitions show some **Q** dependence. In the absence of any detailed calculations, however, we have ignored such effects here. Note that in the present geometry and in the absence of an in-plane (π) polarized component of the incident beam, the resonant scattering measurements are insensitive to the component of the ordered moment along the **b** axis, perpendicular to the scattering plane.

For the scattering arrangement described above, the nonresonant intensity may be written as[22–24]

$$\frac{I}{|f_{\mathrm{mag}}(\mathbf{Q})|^2} \propto \frac{\sin\theta}{\sin 2\theta}\{S_b^2 \sin^2 2\theta + 4\sin^4\theta[S_a \sin\theta + (L_c + S_c)\cos\theta]^2\}. \quad (2)$$

$S_{a,b,c}$ and $L_{a,b,c}$ denote the components of the spin and orbital angular momentum along the corresponding axes, respectively. We assume here that the Ni moments, even if present, make a negligible contribution to the magnetic scattering.[12,26] Therefore, the nonresonant magnetic form factor $f_{\mathrm{mag}}(\mathbf{Q})$ should be determined by the $4f$ electrons of Gd, for which the orbital momentum $L_{a,b,c}$ can be neglected. For our analysis, we have used calculations of the Gd $4f$ magnetic form factor based on a relativistic Dirac-Fock model.[29]

The important point here is that, in contrast to the XRES cross section, nonresonant scattering primarily probes the **b** component of the moment at low-**Q** satellites (small 2θ) and all three components at high-**Q** satellites (large 2θ). Thus, with a judicious choice of satellites, all components of the moment may be studied with a single orientation of the crystal by combining resonant and nonresonant scattering data.

III. RESULTS AND DISCUSSION

Above the Néel temperature, as determined from the magnetization measurements, only charge reflections (h,k,l) with $h+k+l=2n$ were observed. As the temperature was lowered below 19.4 K, additional scattering developed as satellites of the charge peaks at $(h\pm q_a,k,l)$ (Fig. 3) with q_a ranging from 0.550 to 0.553 over the temperature range studied. The equivalence of the $\mathbf{a}^\star$ and $\mathbf{b}^\star$ directions in the tetragonal system also implies the existence of magnetic satellites at $(h,k\pm q_b,l)$ with $q_b = q_a$. However, the alignment of the crystal in the $(h0l)$ zone did not allow us to investigate these peaks. Careful scans along the in-plane and out-of-plane directions did not reveal any additional scattering below 19.4 K that is not associated with the satellite reflections mentioned above.

Figure 4 shows energy scans of the (2,0,0) charge reflection and the $(2-q_a,0,0)$ magnetic satellite across the Gd

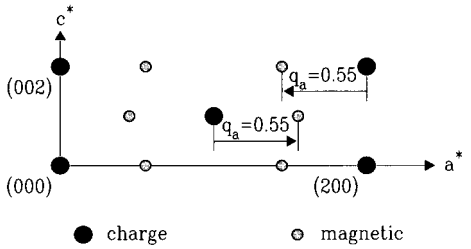

FIG. 3. The $(h0l)$ reciprocal space plane showing the points associated with charge scattering (filled circles), and the points associated with the wave vector of the magnetic modulation $\mathbf{q}_a \approx 0.55\mathbf{a}^\star$ (shaded circles).

$L_{2,3}$ absorption edges at $T = 4$ K. In both cases, the maximum resonant enhancement is observed slightly above the corresponding absorption edge (defined by the maximum slope in the charge reflection data), indicating the electric dipole character of the electronic transitions involved. In the case of electric quadrupole transitions $(2p \leftrightarrow 4f)$ the maximum resonant enhancement is generally observed several eV below the absorption edge[20,21] due to the stronger Coulomb interaction between the $4f$ electrons and the $2p$ core hole. No resonant enhancement was observed at the Gd L_1 edge. All the resonant data presented in this paper were taken at the Gd L_2 resonance where the maximum count rate in the magnetic reflection was achieved. For the ''nonresonant'' scans we chose an incident energy of 7.0 keV, which lies

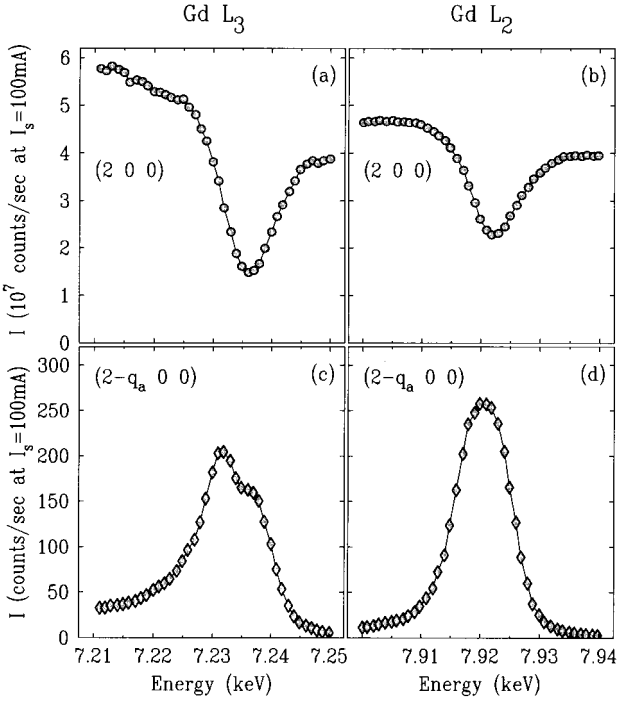

FIG. 4. Energy scans of the (2,0,0) charge (a) and (b) and the $(2-q_a,0,0)$ magnetic reflections (c) and (d) across the Gd L_3 and Gd L_2 absorption edges. In both cases, the maximum resonant enhancement lies slightly above the corresponding absorption edge observed in the charge reflections. This indicates the electric dipole character of the associated electronic transitions.

below all three Gd L absorption edges, to minimize absorption and the fluorescence background. It is worth noting that, although this energy is approximately 200 eV below the L_3 edge, there may still be resonant contributions to the scattering. We estimate that these interference effects are $<4\%$ of the signal, based upon simple numerical models.[20]

Figures 5, 6, and 7 summarize the results of our study of the temperature dependence of the magnetic scattering from $GdNi_2B_2C$. Figures 5 and 6 show selected scans of the nonresonant and resonant scattering at the $(2-q_a,0,0)$ satellite, respectively, while Fig. 7 summarizes the full data set by plotting the position q_a, peak intensity P, and longitudinal width w of the satellite as a function of temperature from fits to the data. Before describing the details of these data and the fits, we point out some of the essential features of the magnetic structure of $GdNi_2B_2C$ as determined by these measurements.

As shown in Figs. 4, 6, and 7, the low-temperature ($T \leqslant 13.6$ K) scans of the $(2-q_a,0,0)$ peak taken at the Gd L_2 energy exhibit a strong resonant scattering contribution. Above approximately 13.6 K, however, the resonant enhancement of the magnetic scattering is essentially absent [see Fig. 7(e)] so that the intensity and line shape of the magnetic scattering observed at the Gd L_2 edge are comparable to the nonresonant data set taken at 7.0 keV. Energy scans showed only a slight resonant enhancement above 13.6 K which we attribute to a small π-polarized component in the incident x-ray beam.[30] The nonresonant magnetic scattering persists up to 19.4 K, the Néel temperature determined from magnetization measurements.

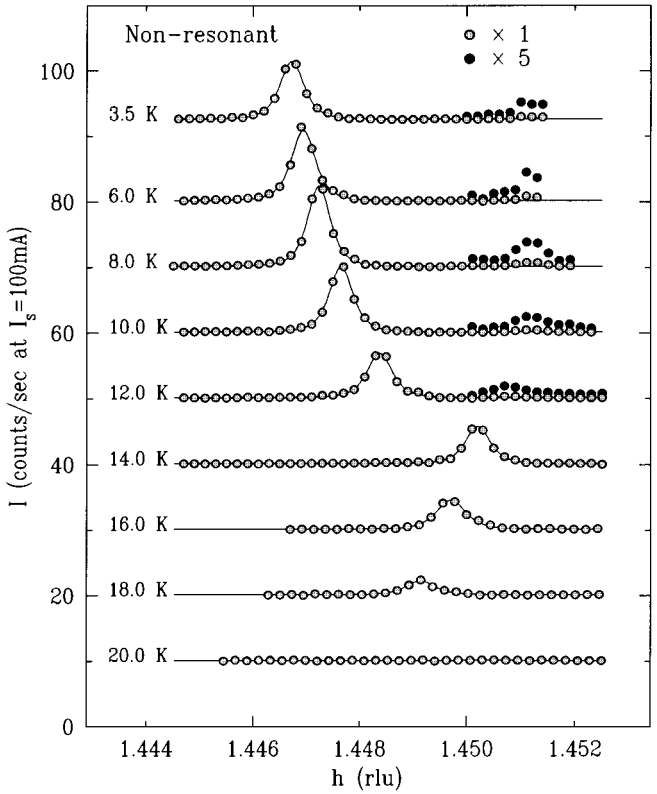

FIG. 5. Selected scans of the measurements of nonresonant magnetic scattering at the $(2-q_a,0,0)$ reflection taken at an energy of 7.0 keV. The lines represent the results of the fits described in the text. To increase the visibility of a second peak, part of the data has been multiplied by 5 (solid circles).

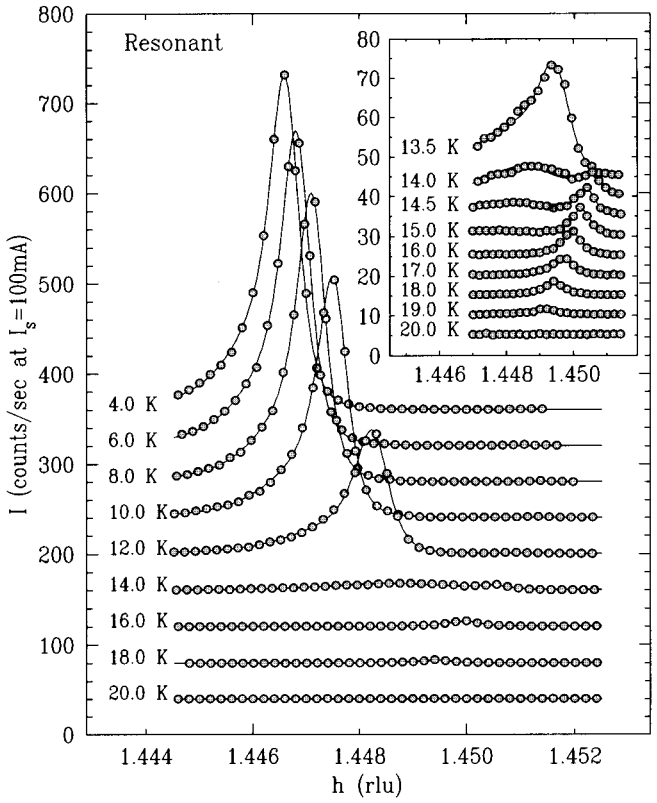

FIG. 6. Selected scans of the measurements of the XRES at the $(2-q_a,0,0)$ magnetic reflection taken at the Gd L_2 absorption edge. The inset shows some of the resonant scans on an expanded intensity scale. Note the presence of a broad and sharp component at 13.5 K, and the reversal in the motion of the magnetic satellite.

From Eqs. (1) and (2), the absence of significant resonant scattering at the magnetic wave vector between 13.6 K and 19.4 K and the presence of nonresonant scattering imply that, in this temperature region, the ordered moment is oriented in

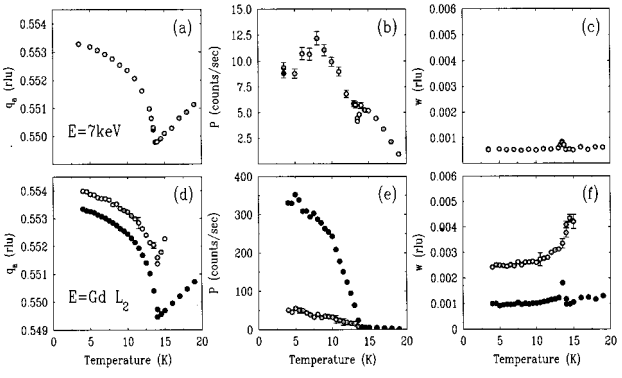

FIG. 7. The results of fits to the complete data set obtained from the nonresonant (a)–(c) and resonant (d)–(f) measurements showing the evolution of position, intensity, and width of these peaks. The transition temperatures observed in the resonant and nonresonant intensities are $T_R = 13.6 \pm 0.1$ K and $T_N = 19.4 \pm 0.3$ K, respectively.

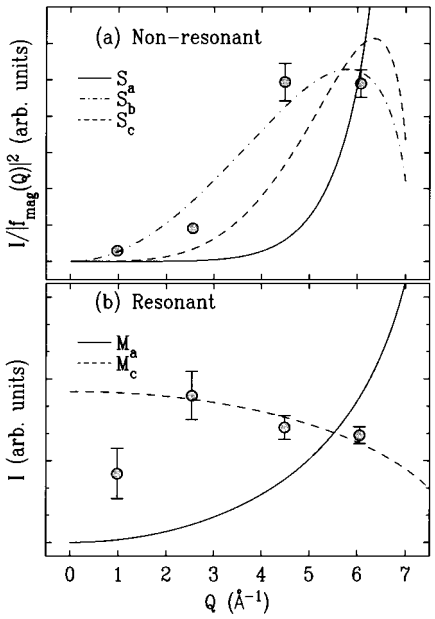

FIG. 8. The **Q** dependence of the integrated intensity of magnetic satellites along the $[h,0,0]$ direction at 3.6 K, obtained off resonance (a) and on resonance (b). The lines show the **Q** dependence of the integrated intensity expected from Eqs. (1) and (2) for ordered components of the Gd $5d$ magnetic moment M and the Gd $4f$ spin S along the **a** (———), **b** (- · - · -), and **c** axis (– – –), respectively.

the basal plane and transverse to the modulation wave vector (e.g., $\mathbf{M}\|\mathbf{b}$ for the **a**-axis modulation), as was found for $ErNi_2B_2C$ by neutron diffraction.[12,13] Below 13.6 K, however, the observation of resonant enhancement implies that an ordered component of the moment exists in the scattering (**a,c**) plane.

In order to determine, more precisely, the direction of the moment below 13.6 K, we have carefully measured the integrated intensity of a series of satellites along the $\mathbf{a}^\star$ axis both on and off the resonance condition at the lowest temperature accessible (3.5 K). To ensure that we actually recorded the full integrated intensity, the analyzer crystal was removed and all slits downstream of the sample were opened until 2θ and χ scans displayed a plateau for all diffraction peaks that were studied. The integrated intensities I measured by rocking the crystal at a fixed scattering angle are shown in Fig. 8. With the exception of the lowest-angle satellite,[31] the **Q** dependence of the resonant scattering [Fig. 8(b)] is well described by a component of the ordered moment along the **c** axis. The **Q** dependence of the nonresonant scattering [Fig. 8(a)] is well described by a component of the moment along the **b** axis.

From these measurements, we deduce that below 13.6 K the moment remains transverse to the propagation direction and acquires a component out of the basal plane. We cannot, however, determine the relative phase shift $\Delta\phi$ between the two components of the moment at low temperature from the present measurements. The magnetic structure may be described in one of two ways, as sketched in Fig. 9:

(a) If the two components are in phase ($\Delta\phi=0$), the structure is a transverse spin modulation as described above

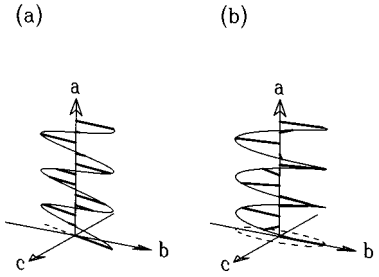

FIG. 9. The two components of the ordered magnetic moment along the **b** and **c** axes feature the same modulation wave vector $\mathbf{q}_a \approx 0.55\mathbf{a}^\star$. However, our measurements did not yield any information on the relative phase shift $\Delta\phi$ between the two oscillations. Two possible structures with $\Delta\phi=\pi$ [spiral-like, (a)] and $\Delta\phi=0$ [transverse wave, (b)] are displayed here.

for 13.6 K $<T<$ 19.4 K, but with the moment rotated away from the **b** axis in the (**b**, **c**) plane (for the modulation along the **a** axis), as shown in Fig. 9(a). In this case, the stronger decrease of the **c** component of the moment with increasing temperature corresponds to a decrease in the angle between the moment and the **b** axis until, at 13.6 K, the moments lock in along the **b** axis.

(b) If the components are out of phase ($\Delta\phi\neq 0$), a modified spiral-like structure results. Different magnitudes of the **b** and **c** components of the spin would lead to an elliptical projection onto the (**b**,**c**) plane [see Fig. 9(b)]. With the disappearance of the **c** component at 13.6 K this structure is degenerate with the planar spin modulation described above. The low symmetry ($2mm$) of the [100] direction is likely to induce fanning or bunching of the spiral which, in turn, will result in a rich spectrum of higher-harmonic satellites. However, the determination of the relative phase $\Delta\phi$ will have to await further measurements of higher harmonic satellites by neutron or XRES experiments.

Having described the basic elements of the magnetic structures observed in $GdNi_2B_2C$ below $T_N=19.4$ K, we briefly discuss some other features found in the XRES and nonresonant scattering data of Figs. 5, 6, and 7.

The nonresonant data are adequately fitted using a Lorentzian-squared line shape. This line shape was chosen simply as an empirical description of the data. The resolution function was not deconvolved from the data. The results of these fits to the nonresonant scattering data are shown in Fig. 7, where we plot the position q_a[7(a)], peak intensity P [7(b)], and longitudinal width, w [7(c)] of the peak.

The fits had to be modified to achieve reasonable agreement with the XRES data. The appearance of two clearly distinguishable peaks between 14 K and 15 K (see the inset in Fig. 6) motivated us to include two peaks in all fits below 15 K, where a single peak was not sufficient to approximate the data. Below 13.6 K, all scans show strongly asymmetric line shapes. The physical reasons for this asymmetry are not fully understood, especially since neither the nonresonant magnetic scattering nor the charge reflections exhibit significant asymmetry. Most likely it is due to strain in the near surface layers. We point out that the resonant scattering measurements are more sensitive to the near surface region as a

result of the strong absorption effects at the L_2 edge. Nevertheless, reasonable fits to the resonant data were achieved by including asymmetry in both peaks. To minimize the number of free parameters, the asymmetry and the background were fixed for all temperatures. The results of these fits are presented in Fig. 7(d), 7(e), and 7(f). The filled circles indicate the position q_{a1}, peak intensity P_1 and longitudinal width w_1 of the first peak, while the shaded circles indicate the corresponding parameters of the second peak. Above 15 K, the intensity of the second peak was constrained to be $P_2=0$.

Figures 7(a) and 7(d) show the magnitude of the modulation wave vector $\mathbf{q}_a$ measured at the $(2-q_a,0,0)$ satellite, as a function of temperature. It decreases with decreasing temperature until, at approximately 13.6 K, this movement reverses direction. Below this temperature, a second reflection with lower, but finite intensity (solid circles in Fig. 5) indicates that a small fraction of the sample does not undergo the second transition at 13.6 K. Instead, the modulation wave vector of these domains continues to decrease with decreasing temperature. The reversal in the motion of the magnetic satellite is reminiscent of what is observed at the transition in pure Er from a **c**-axis-modulated (CAM) structure (with the ordered moment along the **c** axis) above 52 K to a cycloidal structure between 52 K and 18 K, upon the development of a component of the ordered moment in the basal plane.[30,32–34]

Finally, we turn our attention to the transition at 13.6 K. In a narrow range around this temperature, the data taken at the Gd L_2 edge are best characterized by two peaks, one broad and the other sharp, as shown in Figs. 6 and 7. The presence of two peaks in the resonant scattering measurements is reminiscent of earlier measurements[27] of the XRES from $HoNi_2B_2C$. These experiments and theoretical arguments[35] suggest that the origin of a second peak of lower intensity and broader width might be related to structural defects or strain in the ''near surface'' region of the sample.

IV. SUMMARY

Resonant and nonresonant magnetic x-ray scattering techniques have been applied to determine the magnetic structure of $GdNi_2B_2C$. We find that below the Néel temperature, T_N = 19.4 K, the magnetic moments order in a transverse spin modulation with a wave vector $\mathbf{q}_a \approx 0.55\mathbf{a}^*(0.55\mathbf{b}^*)$. A second phase transition occurs at about 13.6 K. Between 19.4 K and 13.6 K, the ordered magnetic moment lies in the basal plane of the tetragonal structure, along the **b**(**a**) axis. In this temperature range, the modulation wave vector decreases with decreasing temperature. Below 13.6 K, an additional component along the **c** direction develops while the modulation wave vector increases with decreasing temperature. Our findings are in good agreement with the magnetization measurements on single crystals described in the Introduction[25] and provide further information about the systematics of magnetic ordering in the RNi_2B_2C family. In particular, the nesting vector close to 0.6 r.l.u. appears to be a general feature of this class of compounds, as predicted by theory.[19]

The authors are grateful to B. N. Harmon, G. H. Lander, Z. A. H. M. Islam, and T. Gu for many useful discussions. Ames Laboratory is operated by the U.S. Department of Energy by Iowa State Universty under Contract No. W-7405-Eng-82. This work was supported by the Director for Energy Research, Office of Basic Sciences. The work at Brookhaven National Laboratory was carried out under Contract No. DE-AC02-76CH00016, Division of Materials Science, U.S. Department of Energy.

[1] R. Nagarajan, C. Maxumundar, Z. Hossain, S. K. Dhar, K. V. Golparrishnan, L. C. Gupta, C. Godart, B. D. Padalia, and R. Vijazarahgavan, Phys. Rev. Lett. **72**, 274 (1994).

[2] R. J. Cava, H. Takagi, H. W. Zandbergen, J. J. Krajewski, W. F. Peck, Jr., T. Siegrist, B. Batlogg, R. B. van Dover, R. J. Felder, K. Mizuhashi, J. O. Lee, H. Eisaki, and S. Uchida, Nature **367**, 252 (1994).

[3] T. Siegrist, H. W. Zandbergen, R. J. Cava, J. J. Krajewski, and W. F. Peck, Jr., Nature **367**, 254 (1994).

[4] R. Cava, H. Takagi, B. Batlogg, H. W. Zandbergen, J. J. Krajewski, W. F. Peck, Jr., R. B. van Dover, R. J. Felder, T. Siegrist, K. Mizuhashi, J. O. Lee, H. Eisaki, S. A. Cater, and S. Uchida, Nature **367**, 146 (1994).

[5] H. Eisaki, H. Takagi, R. J. Cava, K. Mizuhashi, J. O. Lee, B. Batlogg, J. J. Krajewski, W. F. Peck, Jr., and S. Uchida, Phys. Rev. B **50**, 647 (1994).

[6] B. K. Cho, M. Xu, P. C. Canfield, L. L. Miller, and D. C. Johnston, Phys. Rev. B **52**, 3676 (1995).

[7] B. K. Cho, P. C. Canfield, L. Miller, D. C. Johnston, W. P. Beyermann, and A. Yatskar, Phys. Rev. B **52**, 3684 (1995).

[8] K. D. D. Rathnayaka, D. G. Naugle, B. K. Cho, and P. C. Canfield, Phys. Rev. B **53**, 5688 (1996).

[9] B. K. Cho, P. C. Canfield, and D. C. Johnston, Phys. Rev. B **52**, R3844 (1995).

[10] A. I. Goldman, C. Stassis, P. C. Canfield, J. Zarestky, P. Dervenagas, B. K. Cho, D. C. Johnston, and B. Sternlieb, Phys. Rev. B **50**, 9668 (1994).

[11] T. E. Grigereit, J. W. Lynn, Q. Huang, A. Santoro, R. J. Cava, J. J. Krajewski, and W. F. Peck, Jr., Phys. Rev. Lett. **73**, 2756 (1994).

[12] S. K. Sinha, J. W. Lynn, T. E. Girgereit, Z. Hossain, L. C. Gupta, R. Nagarajan, and C. Godart, Phys. Rev. B **51**, 681 (1995).

[13] J. Zarestky, C. Stassis, A. I. Goldman, P. C. Canfield, P. Dervenagas, B. K. Cho, and D. C. Johnston, Phys. Rev. B **51**, 678 (1995).

[14] P. Dervenagas, J. Zarestky, C. Stassis, A. I. Goldman, P. C. Canfield, and B. K. Cho, Physica B **212**, 1 (1995).

[15] P. C. Canfield, B. K. Cho, D. C. Johnston, D. K. Finnemore, and M. F. Hundley, Physica C **230**, 397 (1994).

[16] D. Naugle (unpublished).

[17] B. K. Cho, Ph.D. thesis, Iowa State University, 1995.

[18] B. K. Cho, B. N. Harmon, D. C. Johnston, and P. C. Canfield (unpublished).

[19] J. Y. Rhee, X. Wang, and B. N. Harmon, Phys. Rev. B **51**, 15 585 (1995).

[20] D. Gibbs, D. R. Harshmann, E. D. Isaacs, D. B. McWhan, D. Mills, and C. Vettier, Phys. Rev. Lett. **61**, 1241 (1988).

[21] J. P. Hannon, G. T. Trammel, M. Blume, and D. Gibbs, Phys. Rev. Lett. **61**, 1245 (1988).

[22] F. de Bergevin and M. Brunel, Acta Crystallogr. Sect. A **37**, 324 (1981).
[23] M. Blume, J. Appl. Phys. **57**, 3615 (1985).
[24] M. Blume and D. Gibbs, Phys. Rev. B **37**, 1779 (1988).
[25] P. C. Canfield, B. K. Cho, and K. W. Dennis, Physica B **215**, 337 (1995).
[26] S. L. Bud'ko, M. B. Fontes, D. Aliaga-Guerra, and E. M. Baggio-Saitovitch, Phys. Rev. B **52**, 305 (1995).
[27] J. P. Hill, B. Sternlieb, D. Gibbs, C. Detlefs, A. I. Goldman, C. Stassis, P. C. Canfield, and B. K. Cho, Phys. Rev. B **53**, 3487 (1996).
[28] J. P. Hill and D. F. McMorrow, Acta Crystallogr. Sect. A (to be published).
[29] A. J. Freeman and J. P. Desclaux, Int. J. Magn. **3**, 311 (1972).
[30] M. K. Sanyal, D. Gibbs, J. Bohr, and M. Wulff, Phys. Rev. B **49**, 1079 (1994).
[31] We point out that for both the resonant and nonresonant measurements the lowest- **Q** satellite is subject to the greatest systematic uncertainty since the angle between the incident beam and the sample surface is only about 7°. If the surface of the sample was miscut with respect to the diffracting planes by a small amount (1°–2°), or if the polished surface was rounded, the measured integrated intensity of this peak would strongly decrease. In Fig. 8, the error bars have been approximated by assuming a 2.5° miscut of the sample surface and 5% other systematic errors.
[32] D. Gibbs, J. Bohr, J. D. Axe, D. E. Moncton, and K. L. D'Amico, Phys. Rev. B **34**, 8182 (1986).
[33] R. A. Cowley and J. Jensen, J. Phys. **C 4**, 9673 (1992).
[34] J. Jensen and R. A. Cowley, Europhys. Lett. **21**, 705 (1993).
[35] M. Altarelli, M. D. Núñez-Regueiro, and M. Papoular, Phys. Rev. Lett. **74**, 3840 (1995).